# Innovative Synergistic Control of Electric Fields and $Zn^{2+}$ Dynamics for Revolutionizing Zinc Metal Battery Stability

Shengqiang Zhang[1], Chengxin Liu[2], Yangyang Wang[2], Ao Xu[2], Chunxia Chen[2], Xiaojie Liu[2]*

[1] *School of Chemistry and Chemical Engineering, Yan'an University, Yan'an 716000, China*

[2] *Key Laboratory of Synthetic and Natural Functional Molecule of the Ministry of Education, College of Chemistry & Materials Science, Northwest University, Xi'an 710127, P. R. China*

* Corresponding Author:

E-mail address: xiaojie.liu@nwu.edu.cn (X. Liu)

## Experimental section

### Synthesis of Si@HMCS

Firstly, 0.2 g of silicon powder was oxidized in a muffle furnace at 650 ℃ for 2 h to obtain Si@$SiO_2$. The prepared Si@$SiO_2$ was added to the mixed solution including deionized water (10 mL), anhydrous ethanol (60 mL), and ammonia solution (4 mL), and 4 ml of TEOS was added to the solution after stirring for 3 minutes. Then, a solution containing formaldehyde (0.56 mL) and resorcinol (0.42 g) was added above solution and continued to stir for 48 hours. Finally, Si@$SiO_2$@C was obtained by annealing Si@$SiO_2$@RF at 600 ℃ for 5 h under an argon atmosphere. Typically, Si@$SiO_2$@C was etched by using hydrofluoric acid solution to obtain Si@HMCS.

### Synthesis of F-Si@HMCS

To synthesize F-Si@HMCS, Si@HMCS powder and $NH_4F$ particles were placed in a tubular furnace, positioned downstream and upstream, respectively, at a mass ratio of 5:1. The mixture was then annealed at 300 ℃ for two hours under an $N_2$ atmosphere to complete the process.

### Synthesis of α-$MnO_2$

0.3 g manganese sulfate and 0.23 g potassium permanganate were separately dissolved in 15 mL ultra-pure water, stirred until completely dissolved, transferred to a hydrothermal kettle, hydrothermal reaction at 160 ℃ for 14 h, and then the reaction products were centrifugally washed and dried to obtain pure phase α-$MnO_2$.

### Structural Characterization

The crystalline structure and morphology of samples were analyzed by using X-ray powder diffraction (XRD, Bruker D8 ADVANCE), Scanning electron microscopy (SEM, accelerating voltage: 30 kV, Hitachi SU8010) and Transmission electron microscopy (TEM, Talos F200X, matching with STEM, and EDS mapping). X-ray photoelectron spectroscopy (XPS, PHI5000 VersaProbeIII) was utilized to dissect chemistry states of samples. The specific surface area and pore size distribution of samples were obtained using Brunauer-Emmett-Teller (BET) and calculated using Barrette-Joynere-Halenda (BJH) method. Raman spectroscopy was employed with an

excitation wavelength of 532 nm.

**Electrochemical testing**

CR2025 coin cells were assembled using a glass fiber filter (GF-A, Whatman) as the separator in air to measure the electrochemical performance of samples. The Zn plating/stripping performance was studied in F-Si@HMCS@Zn//F-Si@HMCS@Zn (or bare Zn, Si@HMCS@Zn//Si@HMCS@Zn) symmetric cells. Asymmetrical cells used Cu foil as the cathode and F-Si@HMCS@Zn (or bare Zn, Si@HMCS@Zn) as the anode to analyze the nucleation process and Coulombic efficiency. The aqueous solution of 2 M $ZnSO_4$+0.1 M $MnSO_4$ was used as the electrolyte. The full cells were assembled using $MnO_2$ as the cathodes and the F-Si@HMCS@Zn (or bare Zn, Si@HMCS@Zn) as the anode in the voltage range of 1.0–1.8 V vs. $Zn/Zn^{2+}$ and 0.35–1.4 V vs. $Zn/Zn^{2+}$, respectively. Electrochemical workstation (Chen hua, CHI660E, Shanghai) was used record the LSV, CV, and EIS datas. LSV measurements F-Si@HMCS@Zn (or bare Zn, Si@HMCS@Zn) as the working the counter electrode with the SCE reference electrode in 1 M $Na_2SO_4$. The CV measurement was carried out at different scan rates with the voltage range from 1.0 to 1.8 V for Zn//$MnO_2$ cells. The EIS test was employed in the frequency range of $10^{-2}$–$10^{6}$ Hz.

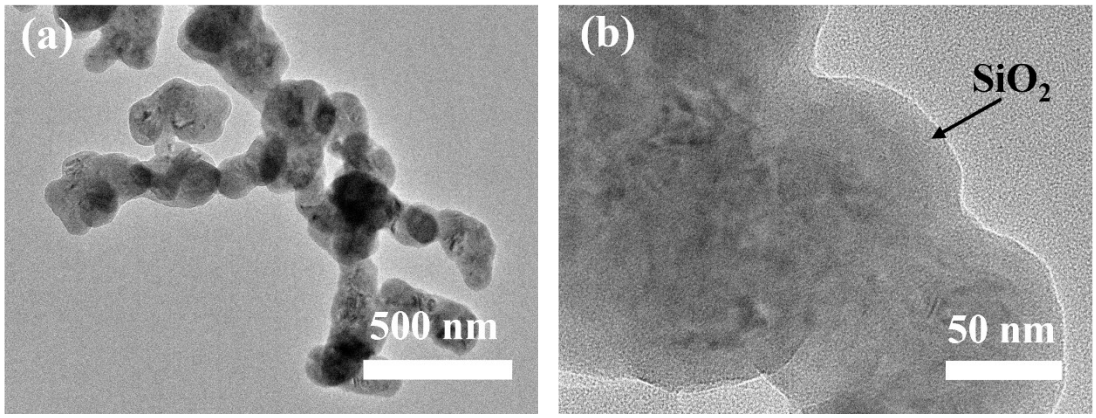


**Fig. S1** (a-b) TEM images of silicon powder after oxidation.

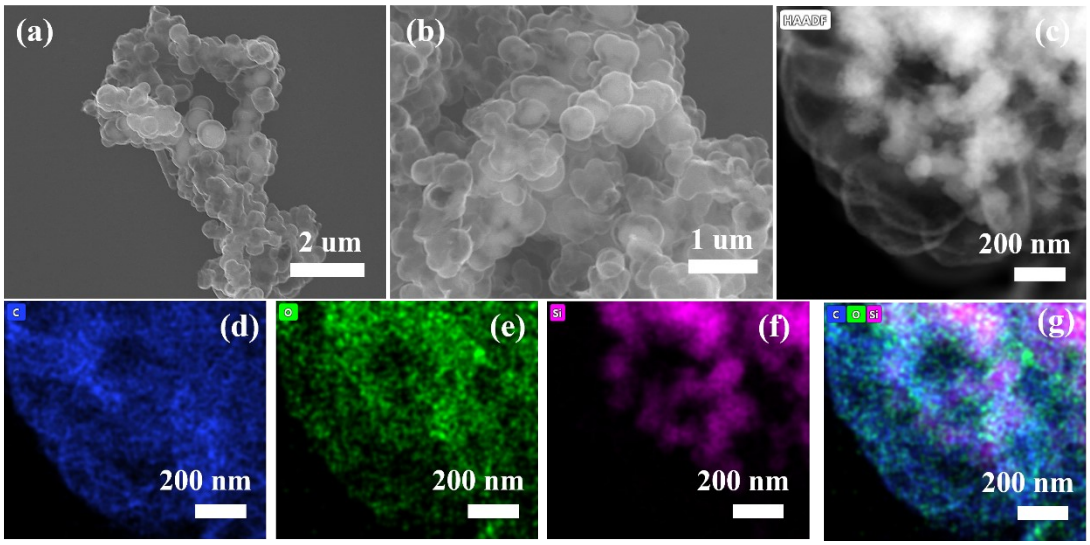


**Fig. S2** (a-b) TEM images of Si@HMCS. (c-g) The elemental mapping images of Si@HMCS.

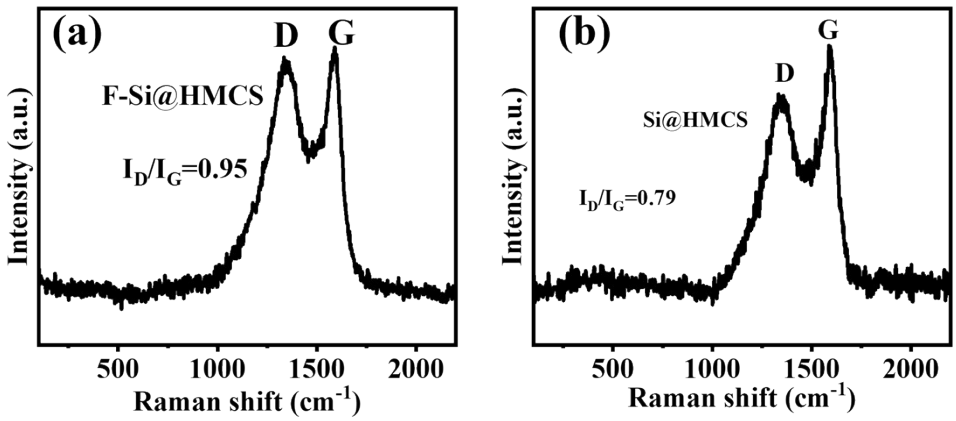


**Fig. S3** Raman spectra of (a) F-Si@HMCS; (b) Si@HMCS.

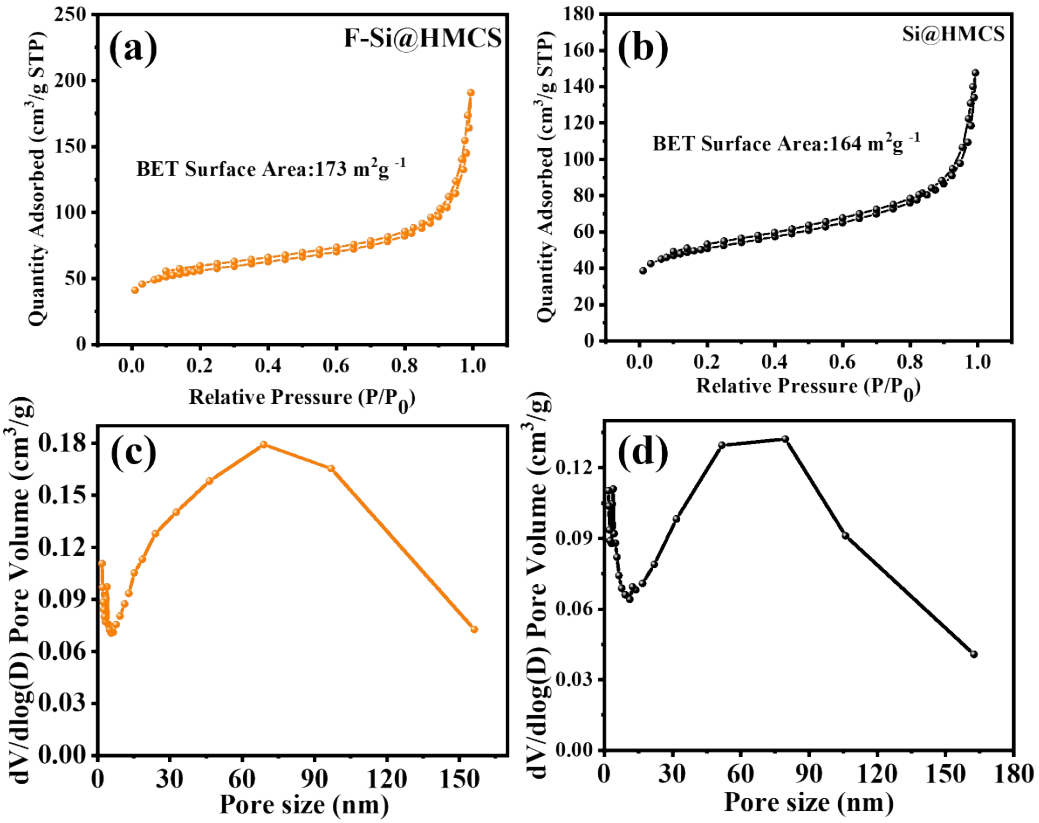


**Fig. S4** The $N_2$ adsorption/desorption isotherm of (a) F-Si@HMCS and (b) Si@HMCS. The corresponding pore-size distribution of (c) F-Si@HMCS and (d) Si@HMCS.

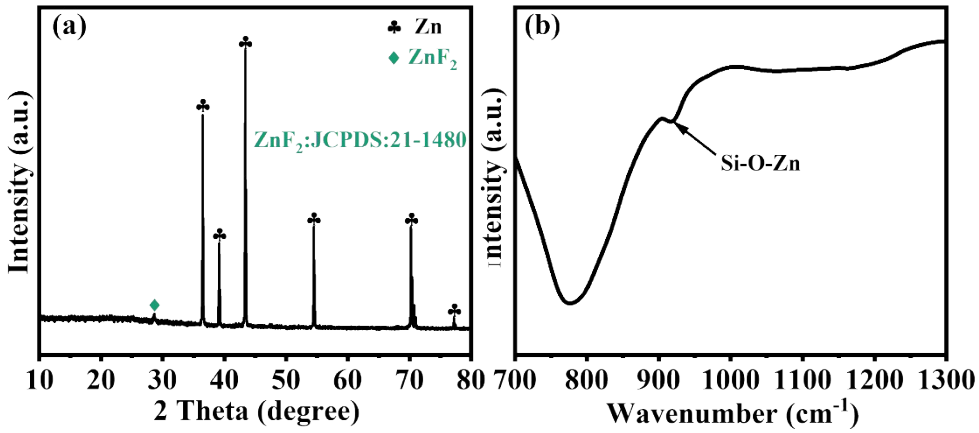


**Fig. S5** (a) XRD pattern of F-Si@HMCS@Zn electrode, (b) FTIR spectra of F-Si@HMCS@Zn electrode

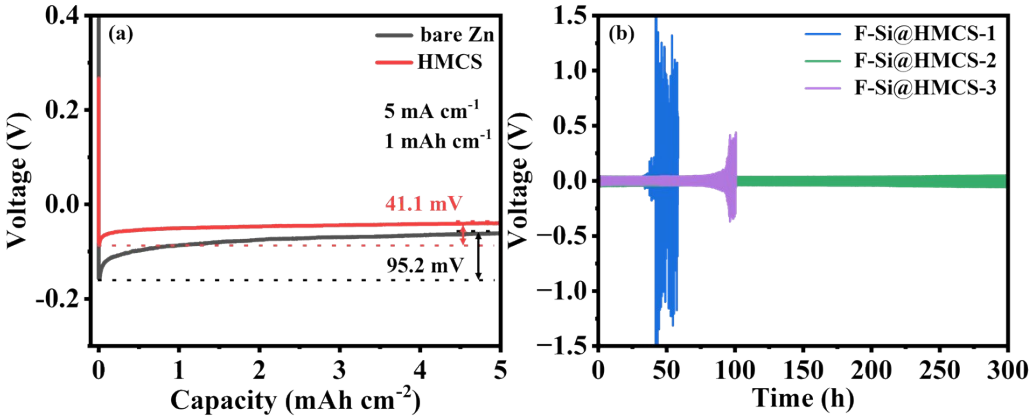


**Fig. S6** (a) Nucleation overpotentials on HMCS@Zn and bare Zn at current density of 5 mA $cm^{-2}$. (b) Long-term cycling performance of F-Si@HMCS-1@Zn, F-Si@HMCS-2@Zn and F-Si@HMCS-3@Zn symmetric cells at current density of 5 mA $cm^{-2}$

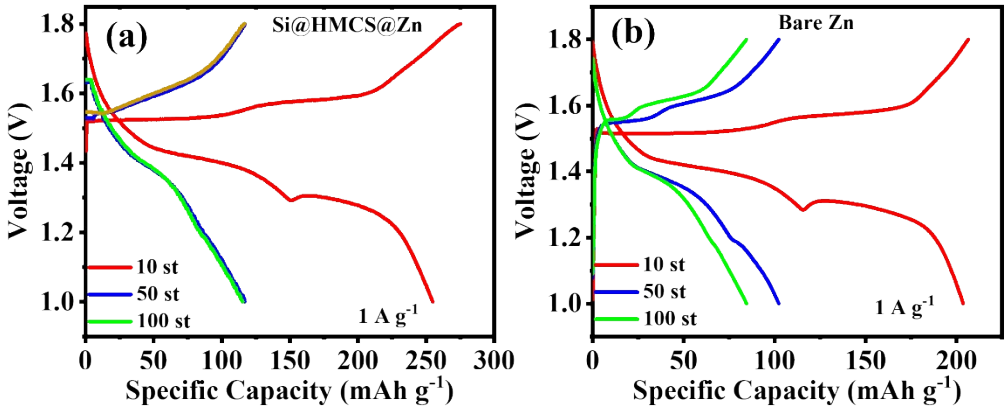


**Fig. S7** The charge-discharge curves of (a) Si@HMCS@Zn//$MnO_2$ and (b) bare Zn//$MnO_2$ after 10, 50, and 100 cycles at 1 A $g^{-1}$

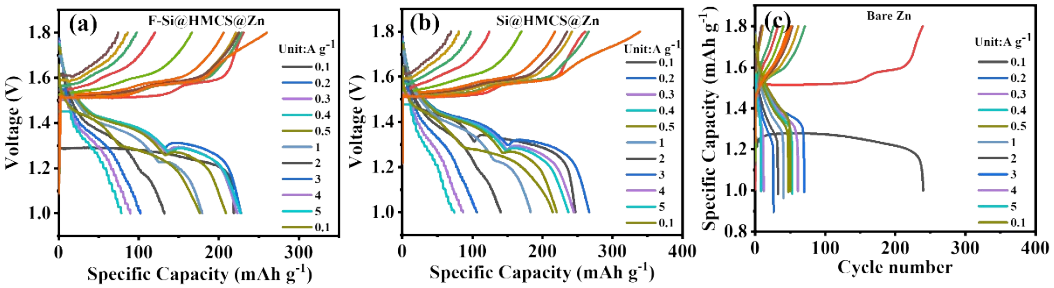


**Fig. S8** charge-discharge profiles of (a) F-Si@HMCS@Zn//$MnO_2$, (b) Si@HMCS@Zn//$MnO_2$, (c) bare Zn//$MnO_2$ at different current densities.

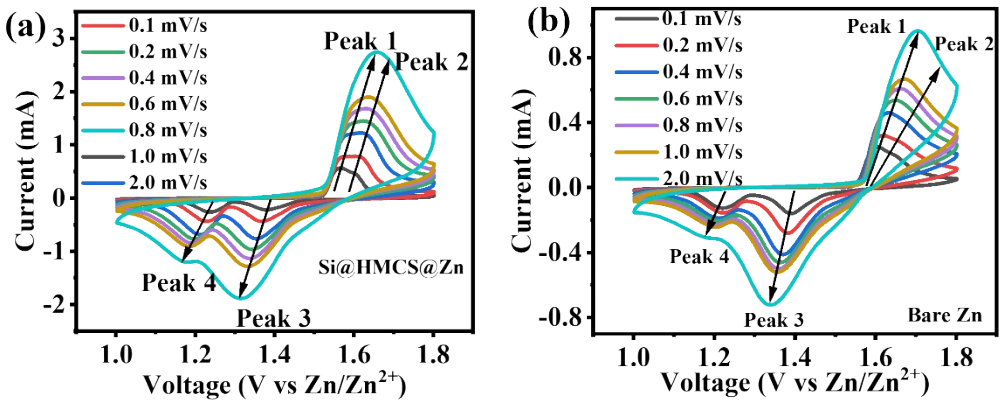


**Fig. S9** CV curve of (a) Si@HMCS@Zn//$MnO_2$ and (b) bare Zn//$MnO_2$ batteries at different scan rates

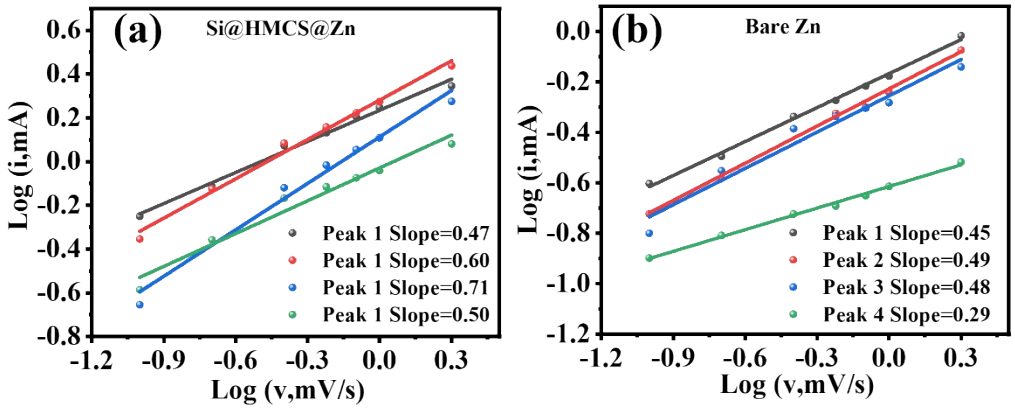


**Fig. S10** Fit plot of log(i) vs. log(v) in peaks 1, 2, and 3 and 4 for (a) Si@HMCS@Zn//$MnO_2$ and (b) bare Zn//$MnO_2$ batteries

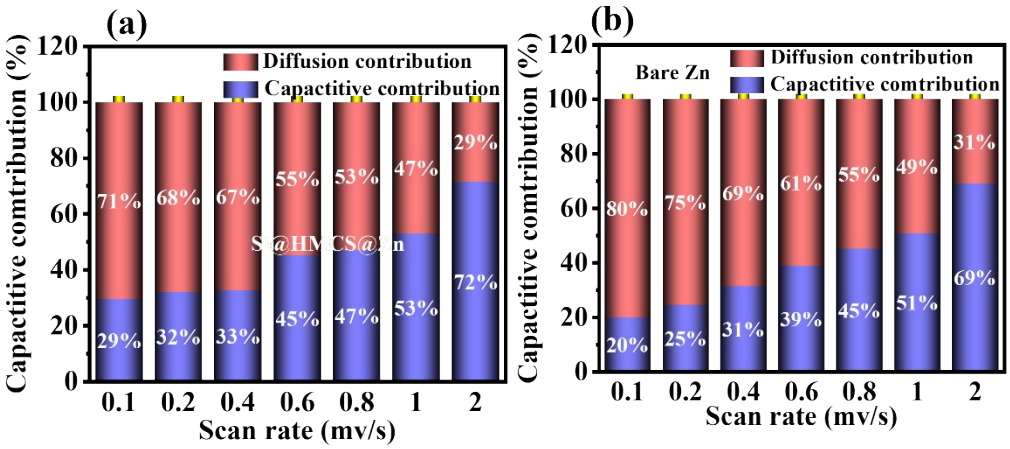


**Fig. S11** Pseudocapacitive contribution plots at different scan rates for (a) Si@HMCS@Zn//$MnO_2$, (b) bare Zn